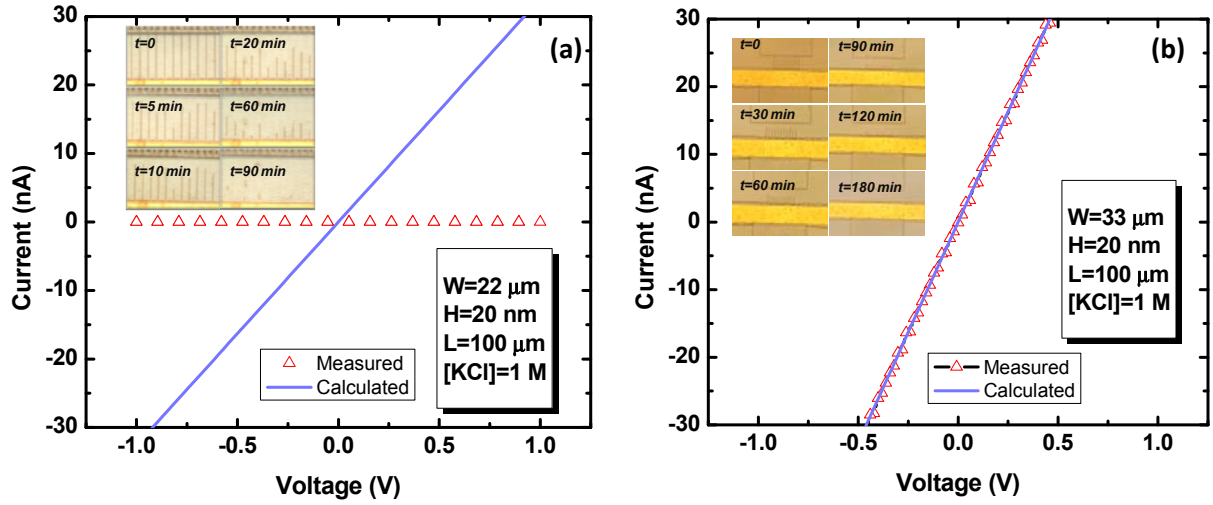
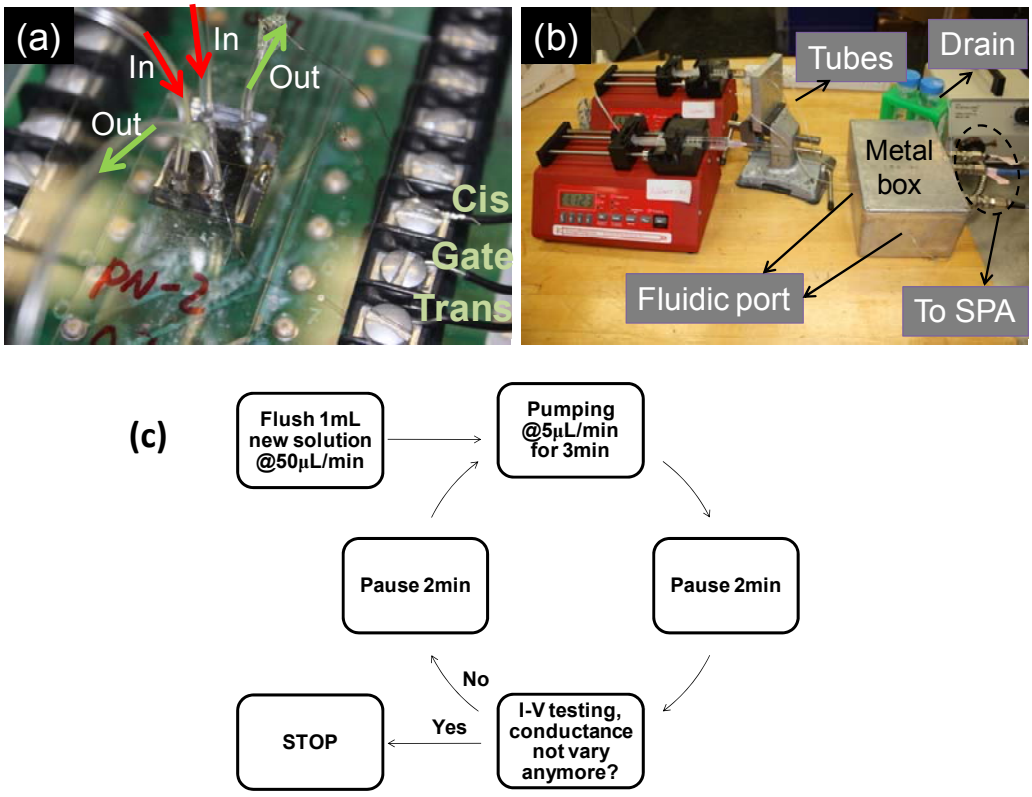
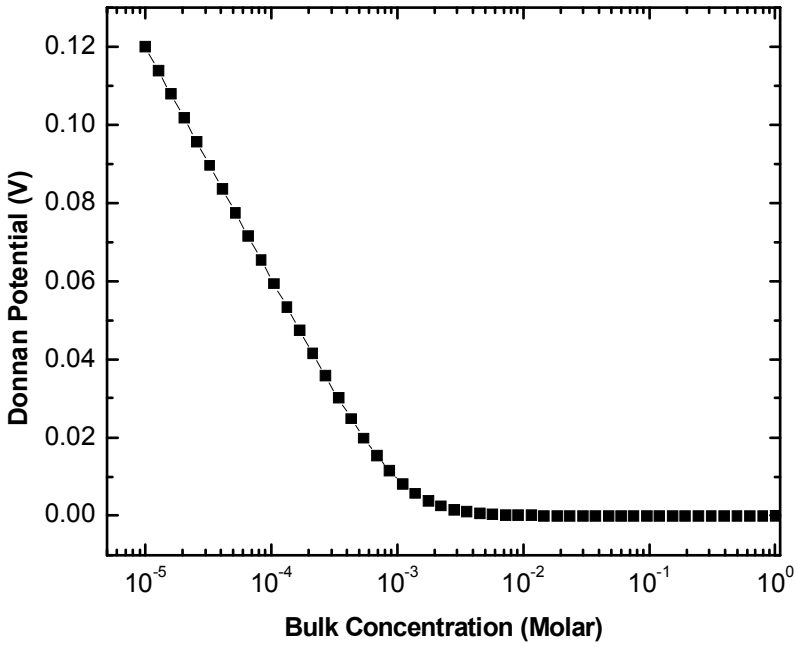
## Supplementary Figures



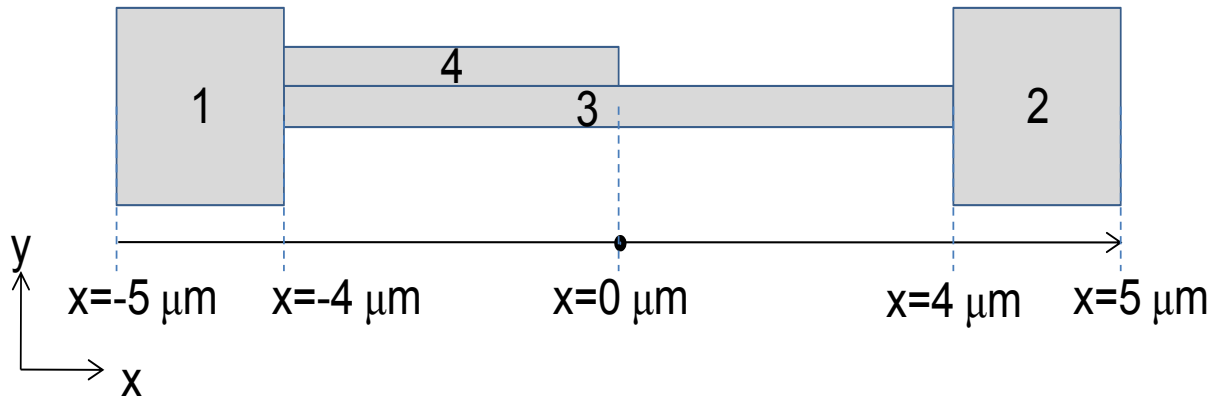

**Supplementary Figure S1 | Comparison between the two different sacrificial layer etching schemes**. **(a)** The current-voltage (I-V) curve for the device fabricated using 'etch and bond' scheme. The inset shows the etching process monitored under the microscope. The measured current is in the order of pico-ampere (pA) and falls very short of the calculated current, which strongly implies a clogged nanochannel. The reasons for the nanochannel collapse may come from two factors, which are the capillary force in the drying process and the pressure exerted during the PDMS bonding process. **(b)** The current-voltage (I-V) curve for the devices fabricated using 'bond followed by etch' scheme. The inset shows the sacrificial layer etching process monitored under the microscope. The measured current agrees very well with calculated current. This confirms the success of the 'bond followed by etch' scheme.



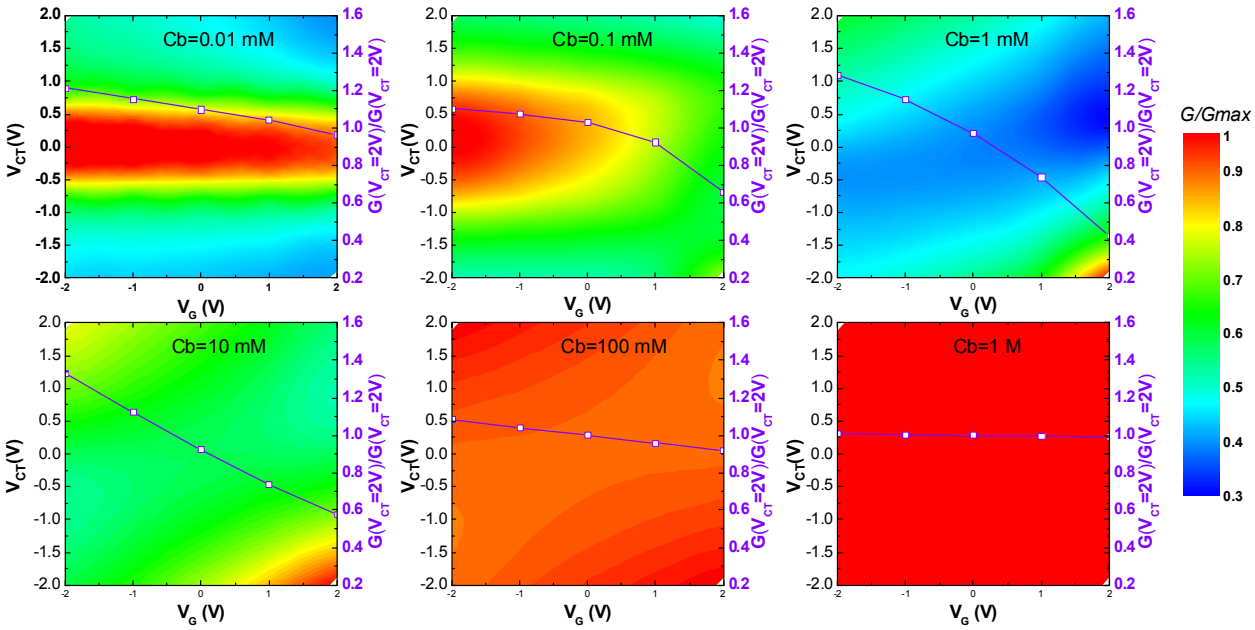

**Supplementary Figure S2 | Experimental setup and schemes of electrical measurements. (a)** The functional device is wire bonded onto a printed circuit board (PCB). The Ag/AgCl electrodes are integrated with the connecting tubes, serving as a low resistive loss contact. **(b)** The whole PCB board is housed inside a light-shielding metal box. The metal box has maximal four BNC connectors (for connection to Cis, Trans and Gate terminals) and four small holes for tubing entering. This setup minimizes the noise from the environment. The whole testing procedure is done using an automatic system. The solutions are delivered by pumps (New Era Pump Systems, Inc) which are controlled by a LabVIEW (National Instruments) program. The current-voltage (I-V) characteristics are measured using HP4156B semiconductor parameter analyzer (SPA). **(c)** Procedure for determining the equilibrium state of a newly introduced solution. When changing concentrations from one value to the other, we always monitor the conductance between the Cis and Trans reservoirs with gate terminal floating. The conductance is determined by a linear fit of the measured current as a function of voltage, scanning from -1 V to 1 V (with a voltage step of 0.1 V and a delay time of 3 s between each measurement point). The equilibrium state for the new solution is reached when the conductance is not changing anymore. And the corresponding experiments are only carried out after this equilibrium state.



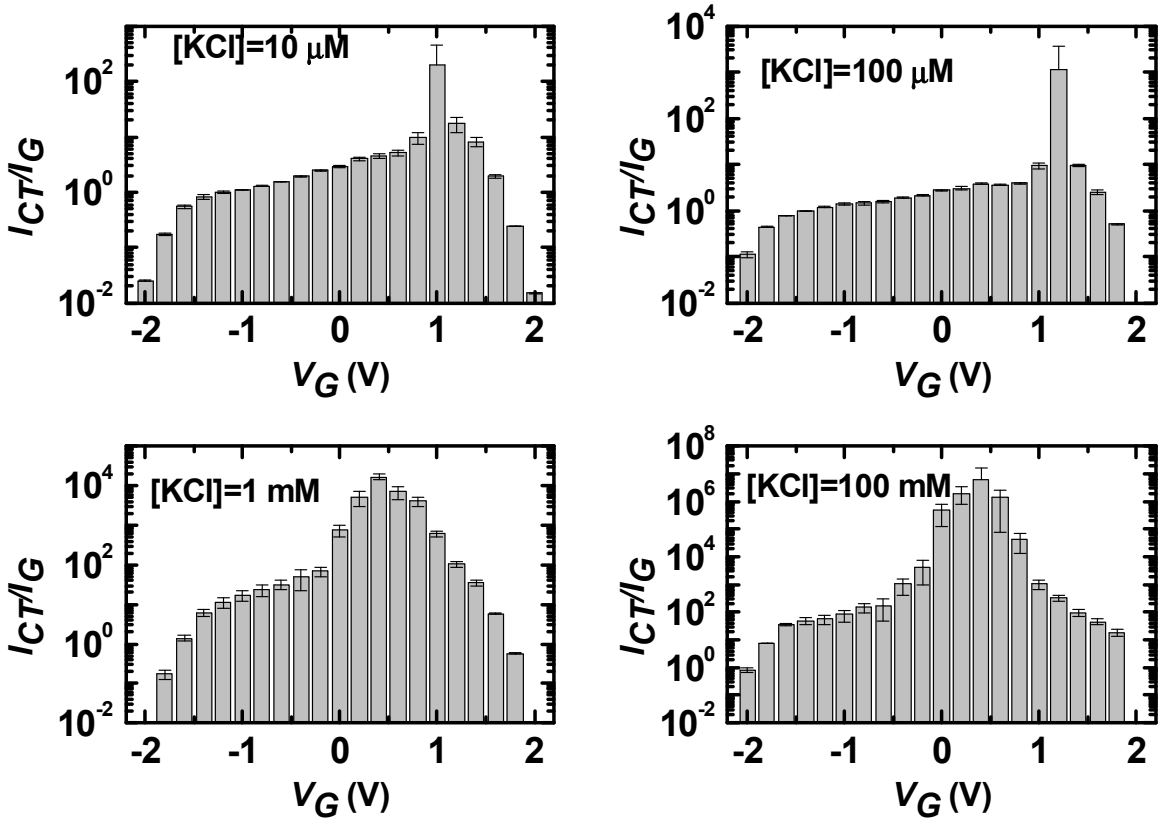

**Supplementary Figure S3** | **The Donnan potential barrier as function of bulk concentration.** When a charge-selective nanochannel is in equilibrium with an adjacent microfluidic reservoir, the electrochemical potentials of the cation (K) or anion (Cl) should be equal in both nanochannels and microchannels. This electrochemical equilibrium is referred to as the Donnan equilibrium. An analogy in semiconductor devices is the aligned Fermi-level. When the Donnan equilibrium of counterions is attained at the microchannel/nanochannel interface, this leads to the Donnan barrier potential at the interface and can be expressed as [34], $V_{bi} = \frac{RT}{F}\ln\frac{[Cl]_n}{C_b} = \frac{RT}{F}\ln\frac{\sqrt{4C_b^2 + s_n^2} + s_n}{2C_b}$, where $R$ [J/(K·mol)] is the universal gas constant, $T$ [K] is the absolute temperature, $F$ [C/mol] is the Faraday constant, $C_b$ [mol/m$^3$] is the bulk concentration. $s_n = 2\sigma_s / ehN_A$ is the nanochannel surface charge density averaged over the channel volume, and $\sigma_s$ is the surface charge density (-2 mC/m$^2$), $h$ is the nanochannel height (20 nm), $N_A$ [mol$^{-1}$] is the Avogadro constant. It can be seen that at high concentrations (>1 mM), this barrier potential is negligible. The maximal barrier happens at low ionic concentrations and is about 0.12 V when the bulk concentration is 10 μM. As a result, this interfacial barrier is a negligible effect in the FERD devices and is not responsible for the voltage tunable rectifying property.



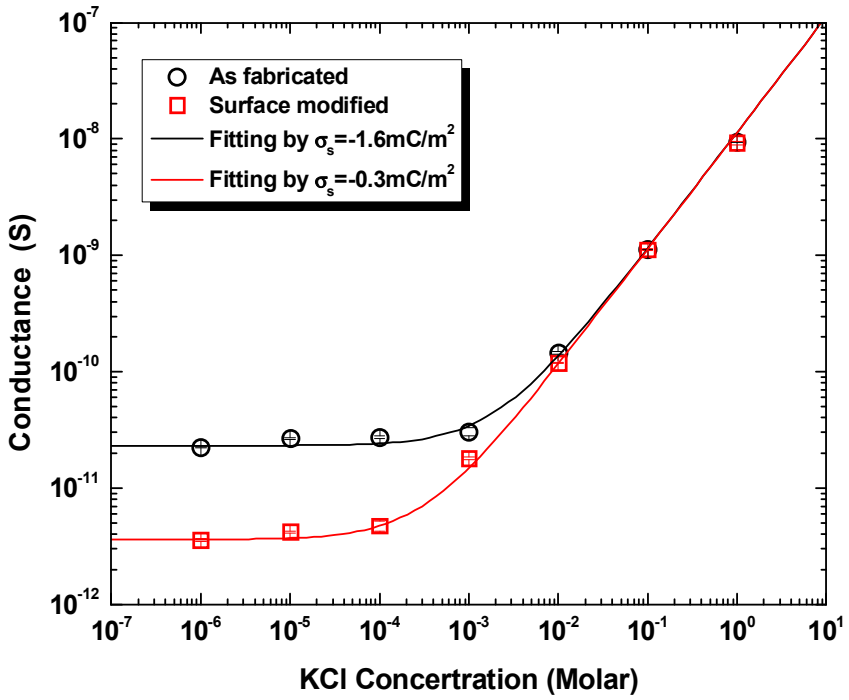

**Supplementary Figure S4 | Simulation system used in the numerical calculation**. It contains an 8-μm-long, 20-nm-high nanochannel (domain 3) connected by two 1×1 $\mu m^2$ square reservoirs (domain 1 and 2). In addition, there is a $SiO_2$ dielectric domain (domain 4) which is 50-nm-thick and 4-μm-long. The length of the nanochannel used for calculation is less than the real device (100 μm) in order to reduce the simulation time. Note the figure is not drawn to scale.




**Supplementary Figure S5 | Normalized nanochannel conductance ($G/G_{max}$) as a function of $V_G$ and $V_{CT}$ for various bulk concentrations ($C_b$).** The inset lines are the rectifying ratio at $V_{CT}$=±2 V. The asymmetry of the surface plot about the $V_{CT}$=0 indicates a rectifying property. It can be seen that the gate voltage tunable rectifying property is most prominent at intermediate ion concentrations (e.g. 1 mM and 10 mM), and is weakened at both low and high ionic concentrations. The general dependence of the rectifying degree on the gate potential and the bulk concentrations agrees very well with the experimental data shown in Figure 5 in the main text.




**Supplementary Figure S6 | Gate Leakage considerations.** Besides the capacitive coupling between the gate electrodes and the liquid nanochannel, the real dielectric is lossy and therefore a leakage current usually exists. We always monitor the gate leakage current ($I_G$) during the measurement. The figure of merit that we use to tell whether the gating effect is dominated by capacitive coupling or leakage coupling is by looking at the ratio of $I_{CT}$ over $I_G$. If this ratio is less than 1, then the device has a significant amount of leakage current through the gate dielectric. To obtain a trustable capacitive gating results, we need $I_{CT}/I_G$ to be larger than 1. This ratio is both gate voltage dependent and KCl concentration dependent. At high KCl concentrations, $I_{CT}/I_G$ is usually very large because of the large $I_{CT}$ flowing in the channel. However, at low KCl concentrations, the leakage current flowing between the nanochannel and the gate electrode can exceed $I_{CT}$. Nevertheless, $I_{CT}/I_G$ is usually larger than 1 when the gate voltage is bounded between -1.5 V and 1.5 V, and this is a typical safe gate voltage range used in our experiments. The error bar corresponds to 10 measurements.




**Supplementary Figure S7 | Measured conductance as a function of KCl concentrations for the nanochannel before and after surface modification.** This dimensions for this nanochannel are *W*=11 μm, *L*=116 μm, *H*=8 nm. The surface charge is reduced from an intrinsic value of -1.6 mC/m$^2$ to -0.3 mC/m$^2$ after the modification.

## Supplementary Table

**Supplementary Table S1**. Parameters used in the numerical simulation.

| Parameters | Meaning | Value | Unit |
|---|---|---|---|
| $\varepsilon_0$ | Vacuum permittivity | 8.85e-12 | F/m |
| $\varepsilon_{SiO_2}$ | PECVD $SiO_2$ dielectric constant [43] | 5 | No unit |
| $\varepsilon_w$ | KCl solution dielectric constant [44] | 70 | No unit |
| $\sigma_s$ | Intrinsic surface charge | -2e-3 | $C/m^2$ |
| $\varphi$ | Potentials in gate dielectric | | V |
| $c_i$ | Concentration of ionic species *i* | | $mol/m^3$ |
| $C_b$ | Bulk concentration | Variables | mM |
| $D_i$ | Diffusion coefficient | 1.96e-9 ($K^+$), 2.03e-9 ($Cl^-$) | $m^2/s$ |
| $F$ | Faraday constant | 96485.3415 | s·A/mol |
| $i$ | Ion species | 1 ($K^+$), 2 ($Cl^-$) | No unit |
| $I$ | Total current | | A/m |
| $I_i$ | Ionic current of $i^{th}$ species | | A/m |
| $n$ | Normal vector | | |
| $N_i$ | Mass flux density of $i^{th}$ species | | $mol/(m^2 \cdot s)$ |
| $u_i$ | Ionic mobility of $i^{th}$ species | 7.62e-8 ($K^+$), 7.92e-8 ($Cl^-$) | $m^2/(V \cdot s)$ |
| $V$ | Potentials in the liquid | | V |
| $V_C$ | Potential in the Cis reservoir | variables | V |
| $V_T$ | Potential in the Trans reservoir | variables | V |
| $V_G$ | Gate potential | variables | V |
| $z_i$ | Charge number | +1 ($K^+$), -1($Cl^-$) | No unit |

## Supplementary Methods

### 'Etch and bond' approach

In this approach, the diced devices are firstly immersed in a chrome etchant solution (Transene, type 1020) heated at 70 °C, and the etching process is monitored under a microscope. A total time of 90 min is enough to remove the entire Cr sacrificial layer (vertical lines in the inset image of Supplementary Figure S1a). After the Cr layer is etched away, the device is rinsed with de-ionized (DI) water and dried in an oven. After that the surface of both the device and the PDMS stamp are treated with oxygen plasma and they are bonded together. It is during this bonding process that a certain pressure is needed to press these two pieces together. After the device is integrated, we carry out experiments to see whether the nanochannel functions correctly. 1 M KCl solutions are introduced into the microchannels and the Cis to Trans current is measured as a function of Cis to Trans voltage (Supplementary Figure S1a).

### 'Bond followed by etch' approach

To overcome the collapse problem encountered in the 'etch and bond' approach, we develop a new scheme to remove the sacrificial layer. The diced device and the PDMS stamp are firstly treated with oxygen plasma. Then we bond these two pieces together. Connecting tubes are inserted into PDMS inlet and outlet ports. Subsequently, DI water is pumped along the microchannel to wet the Cis/Trans reservoirs. Then the chrome etchant (Transene, type 1020) is pumped along the microchannel and it diffusively etches the embedded sacrificial Cr layer *in situ*. The inset images of Supplementary Figure S1b shows the etching process using this new approach. After the etching process being completed, DI water is flushed along the microchannels to rinse the channel. 1 M KCl solutions are introduced into the device and the I-V properties between the Cis and Trans reservoirs are tested (Supplementary Figure S1b).

### Determination of the surface charge density

The conductance of a nanochannel filled with KCl solutions is the superposition of the bulk conductance $e(\mu_K+\mu_{Cl})C_bN_AWH/L$ and the double layer conductance $2\mu_K\sigma_SW/$L, where $W$ [m], $L$ [m] and $H$ [m] are the width, length and height of the nanochannels, respectively. $\mu_K$ [$m^2/(V\cdot s)$] and $\mu_{Cl}$ [$m^2/(V\cdot s)$] are the mobility of K and Cl ions. $C_b$ [$mol/m^3$] is the bulk concentration. $N_A$ [$mol^{-1}$] is the Avogadro constant, $e$ [C] is the elementary charge. $\sigma_S$ [$C/m^2$] is the surface charge on the nanochannel walls. By knowing the

dimensions of the lithographically defined channels (*W, L*), we can derive the value of *H* in high concentration regime (bulk conductance part) and the value of surface charge $\sigma_S$ in low concentration regime (double layer conductance part) by fitting the experimental data.

**Numerical calculation**

The steady-state distributions of the cation/anion concentration and the ionic current under different $V_G$ and $V_{CT}$ biases are calculated by solving the coupled two dimensional (2D) Poisson-Nernst-Planck (PNP) equations using COMSOL script environment. Supplementary Figure S4 shows the system that we use in the simulation.

We use three modules in the COMSOL environment: Electrostatics (AC/DC Module), Nernst-Planck without electroneutrality for calculation of $K^+$ ions (Chemical Engineering Module) and Nernst-Planck without electroneutrality for calculation of $Cl^-$ ions (Chemical Engineering Module). The governing equations and the corresponding boundary conditions are listed as follows (Supplementary Table S1 summarizes all the parameters used in the simulation),

A. Electrostatics

(1) Governing equations (Poisson equation):

$\varepsilon_0\varepsilon_w\nabla^2 V = -\sum_i Fz_i c_i$ for domain 1, 2 and 3, and

$\varepsilon_0\varepsilon_{SiO_2}\nabla^2\varphi = 0$ for domain 4.

(2) Boundary conditions:

The Dirichlet boundary condition is used for the potentials at the ends of the two reservoirs, $V(x=-5\mu m)=V_C$ and $V(x=5\mu m)=V_T$. The gate electrode (top side of domain 4) has Dirichlet boundary condition as $V=V_G$. Neumann boundary conditions are applied for all the other reservoir walls, $-\varepsilon_0\varepsilon_w n\cdot\nabla V=0$. The nanochannel walls which are not in contact with the gate dielectric have the boundary condition as $-\varepsilon_0\varepsilon_w n\cdot\nabla V=\sigma_s$. The Neumann boundary condition is imposed on the interface between the gate dielectric and nanochannel as $-\varepsilon_0\varepsilon_w n\cdot\nabla V+\varepsilon_0\varepsilon_{SiO_2} n\cdot\nabla\varphi=\sigma_s$.

B. Steady state Nernst-Planck equation for either $K^+$ or $Cl^-$

(1) Governing equations:

$\nabla \cdot N_i = \nabla \cdot (-D_i \nabla c_i - z_i u_i c_i \nabla V) = 0$ for domain 1, 2 and 3, and inactive in domain 4.

(2) Boundary conditions:

The Dirichlet boundary condition is used for the ionic concentrations at the ends of the two reservoirs, $c_i(x = \pm 5\mu m) = C_b$. The normal ionic fluxes through all the other walls are set to be zero, $n \cdot N_i = 0$.

After solving the coupled PNP equations, the ionic concentration and potential distributions can be extracted. The resulting ionic current $J_i$ of $i^{th}$ species through the nanochannel can be integrated as, $J_i = \int z_i F N_i dS$, where $S$ is a cross-sectional area of the nanochannel. The total ionic current can thus be obtained as $J = \sum_i J_i$. The averaged $K^+$ and $Cl^-$ concentrations along the *x* direction is calculated by $< c_i(x) >= \int_{y=-H/2}^{y=H/2} c_i(x,y)dy / H$, where $H$ is the channel height.

**Derivations of $\rho_K$ and $\rho_{Cl}$**

For the un-gated area (subscript T), according to the charge neutrality condition, we can obtain,

$$[K]_T - [Cl]_T = \frac{2\sigma_s}{ehN_A} \qquad \text{(S1)}$$

According to the law of the conservation of mass, we obtain the other relationship,

$$[K]_T [Cl]_T = C_b^2 \qquad \text{(S2)}$$

Therefore, the averaged cation/anion concentrations under the un-gated area can be determined as,

$$[K]_T = -\frac{s_T}{2} + \sqrt{(\frac{s_T}{2})^2 + C_b^2} \quad \text{and} \quad [Cl]_T = \frac{s_T}{2} + \sqrt{(\frac{s_T}{2})^2 + C_b^2} \qquad \text{(S3)}$$

where $s_T = 2\sigma_s / ehN_A$ is the surface charge concentration. As a result,

$$\gamma_T \equiv \frac{[K]_T}{[Cl]_T} = \frac{(-s_T + \sqrt{s_T^2 + 4C_b^2})^2}{4C_b^2} \qquad \text{(S4)}$$

For the gated area, it is reasonable to assume that all the gate voltage is dropped on the gate dielectric. According to the charge neutrality condition, we can get,

$$[K]_C - [Cl]_C = \frac{2\sigma_s - \varepsilon_0 \varepsilon_{SiO2} V_G / d_{SiO2}}{ehN_A} \quad \text{(S5)}$$

By applying the law of the conservation of mass, we obtain,

$$[K]_C [Cl]_C = C_b^2 \quad \text{(S6)}$$

Therefore, the averaged cation/anion concentrations under the gated area can be determined as,

$$[K]_C = -\frac{s_C}{2} + \sqrt{(\frac{s_C}{2})^2 + C_b^2} \quad \text{and} \quad [Cl]_C = \frac{s_C}{2} + \sqrt{(\frac{s_C}{2})^2 + C_b^2} \quad \text{(S7)}$$

where

$$s_C = \frac{2\sigma_s - \varepsilon_0 \varepsilon_{SiO2} V_g / d_{SiO2}}{ehN_A} \quad \text{(S8)}$$

As a result,

$$\gamma_C \equiv \frac{[K]_C}{[Cl]_C} = \frac{(-s_C + \sqrt{s_C^2 + 4C_b^2})^2}{4C_b^2} \quad \text{(S9)}$$

According to the total current continuity at the micro/nano channel interfaces in the Trans side, we obtain,

$$J_T^K - J_T^{Cl} = J_{TBluk}^K - J_{TBluk}^{Cl} \quad \text{(S10)}$$

$J_{TBluk}^K$ and $J_{TBluk}^{Cl}$ is the K and Cl current flux in the Trans reservoir and can be assumed to have the relation of $J_{TBluk}^K = -J_{TBluk}^{Cl}$ because of an equal K and Cl concentration and a similar K and Cl mobilities in the bulk. Moreover, it is easy to see that in the nanochannel, $J_T^K / J_T^{Cl} = -[K]_T / [Cl]_T = -\gamma_T$, therefore,

$$J_T^K / J_{TBulk}^K = 2/(1+\gamma_T^{-1}) \quad \text{(S11)}$$

$$J_T^{Cl} / J_{TBulk}^{Cl} = 2/(1+\gamma_T) \quad \text{(S12)}$$

Similarly, we get the following relationship at the interface of Cis reservoir and the nanochannel ,

$$J_C^K / J_{CBulk}^K = 2/(1+\gamma_C^{-1}) \quad \text{(S13)}$$

$$J_C^{Cl} / J_{CBulk}^{Cl} = 2/(1+\gamma_C) \quad \text{(S14)}$$

It is easy to see that $J_{TBulk}^K = J_{CBulk}^K$ and $J_{TBulk}^{Cl} = J_{CBulk}^{Cl}$. Therefore, we can obtain the ratios of cation (anion) flux via the Cis side over the cation (anion) flux via the Trans side of the nanochannel as,

$$\rho_K \equiv \frac{J_C^K}{J_T^K} = \frac{1+\gamma_C^{-1}}{1+\gamma_T^{-1}} \quad \text{(S15)}$$

$$\rho_{Cl} \equiv \frac{J_C^{Cl}}{J_T^{Cl}} = \frac{1+\gamma_C}{1+\gamma_T} \quad \text{(S16)}$$

**Surface charge modification**

By neutralizing the intrinsic surface charge through chemical modifications, it would allow for more efficient gate modulation of the cation/anion concentration inside the nanochannel. The procedure we used in the surface charge modification is as follows.

1. Flushing the microchannel with ethanol (Sigma-Aldrich, category # 459836) for 3 hours.

2. Flushing the microchannel with 2% v/v 3-Glycidoxypropyltrimethoxysilane (GPTS) (Sigma-Aldrich, category # 440167) in ethanol (Sigma-Aldrich, category # 459836) for 3 hours.

3. Flushing the microchannel with 50 mM ethanolamine (Sigma-Aldrich, category # 411000) for 1.5 hours.

## Supplementary References

43. Schwartz, G. C., Huang, Y. S. & Patrick, W. J. The Effective Dielectric-Constant of Silicon Dioxides Deposited in the Spaces between Adjacent Conductors. *J. Electrochem. Soc.* **139**, L118-L122 (1992).

44. Chandra, A. Static dielectric constant of aqueous electrolyte solutions: Is there any dynamic contribution? *J. Chem. Phys.* **113**, 903-905 (2000).